Nanoscale

ROYAL SOCIETY OF CHEMISTRY

PAPER

View Article Online
View Journal | View Issue

Check for updates

Cite this: *Nanoscale*, 2022, **14**, 7269

Nonlinear plexcitons: excitons coupled with plasmons in two-photon absorption†

Yichuan Chen, Yuqing Cheng and Mengtao Sun *

Received 13th December 2021,
Accepted 11th April 2022

DOI: 10.1039/d1nr08163b

rsc.li/nanoscale

The nonlinear optical properties of a D–A (donor–acceptor) conjugated organic molecule with polythiophene (PT) as the donor and indene-C_{60} bisadduct ($IC_{60}BA$) as the acceptor are theoretically investigated, which exhibits a large two-photon absorption (TPA) cross-section up to 8000 GM at the wavelength of 780 nm. Combining surface plasmon resonances (SPRs) with nonlinear optics, nonlinear properties can be strongly enhanced. In this paper, an appropriate nonlinear plexciton method by the coupling of Au@Ag nanorods and an Ag film is designed, in which the TPA properties of the PT:$IC_{60}BA$ complex can be increased by 10^6 times. The angle dependence on polarization and incidence is investigated to obtain the maximum of plasmonic enhancement. Our results emphasize the physical mechanism of nonlinear plexcitons and provide a feasible method to improve the nonlinear properties of organic solar cell materials.

Published on 11 April 2022. Downloaded on 12/26/2025 10:37:54 AM.

1. Introduction

The development of ultrafast lasers promotes the research of nonlinear optics.[1–7] Two-photon absorption (TPA) is a nonlinear absorption process.[8] The discussion of TPA can be traced back to Göppert-Mayer's doctoral thesis in the 1930s,[9] and practical experiments were carried out in the 1960s.[10] Because of its high photon density and low light damage, TPA has wide applications in optical data storage,[11] microprocessors,[12,13] photodynamic therapy,[14,15] *etc.* However, TPA effects are usually weak as the reaction probability depends on square irradiance, which limits its optical performance. Recently, researchers combined the subwavelength electromagnetic field confinement properties of surface plasmon resonances (SPRs) with nonlinear optics, enabling weak nonlinear effects to be enhanced in micro–nano structures, and forming a new research field, named nonlinear surface plasmonic photonics.[16] The localized electric field associated with localized surface plasmon resonances (LSPRs) can be intense enough to strongly modify the nonlinear properties near the surface of metallic nanoparticles. A prime instance is surface enhanced Raman scattering (SERS), where plasmonic excitations can enhance the inherently weak Raman scattering by orders of magnitude, even allowing for single-molecule detection.[17] The plasmonic method can also work for enhancing the TPA response of molecules. Therefore, a plausible conjecture lies in the plasmonic-enhanced TPA properties of solar cells.

Applying TPA to solar cells is promising because it offers an attractive possibility to overcome the Shockley–Queisser limit.[18] Thus, it has generated a demand for developing solar cell materials with large TPA cross-sections. The research of organic TPA materials is the frontier of nonlinear optical materials.[19,20] Organic molecules with conjugated structures are more prone to polarization in solar light, and their broad-spectrum absorption and efficient light-harvesting satisfy the TPA process.[21–23] Therefore, for the selection of TPA organic solar cell (OSC) materials, fullerenes and their derivatives are appropriate. A polythiophene:indene-C_{60} bisadduct (PT:$IC_{60}BA$) donor–acceptor (D–A) complex with polythiophene (PT) as the donor and indene-C_{60} bisadduct ($IC_{60}BA$) as the acceptor was selected in our theoretical study. Such bulk-heterojunction polymer OSCs have attracted more and more attention owing to their high carrier mobility and strong absorption in the visible region.[24,25] Fig. 1 shows the molecular structures of PT and $IC_{60}BA$. Considering their distinct conjugated systems, especially $IC_{60}BA$ as a fullerene derivative, the PT:$IC_{60}BA$ complex may exhibit significant nonlinear optical properties.

Constrained by unobvious optical nonlinearity, direct application of TPA materials to solar cells performs poorly. How to improve the nonlinear properties of materials has become a hot issue.[26] One such concept is intermediate band (IB) solar cells, in which the TPA process involves a partially occupied IB that works as a "stepping stone" for optical transitions.[27] IB solar cells can be achieved through quantum dots and highly

School of Mathematics and Physics, Beijing Advanced Innovation Center for Materials Genome Engineering, University of Science and Technology Beijing, Beijing 100083, China. E-mail: mengtaosun@ustb.edu.cn

† Electronic supplementary information (ESI) available. See DOI: https://doi.org/10.1039/d1nr08163b

Published on 11 April 2022. Downloaded on 12/26/2025 10:37:54 AM.

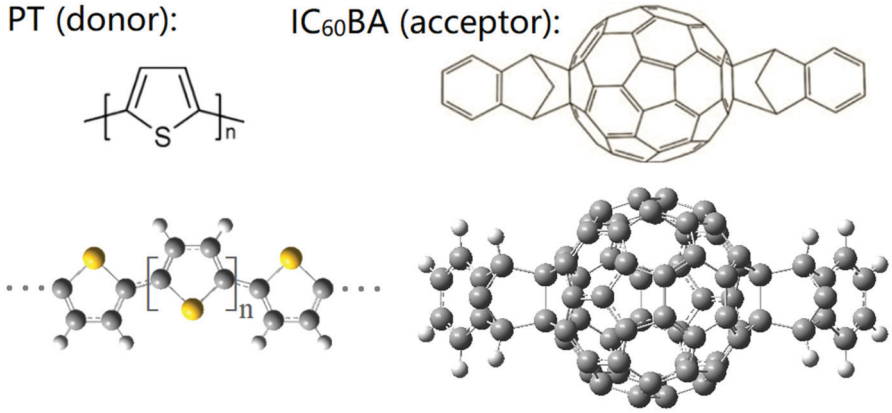

Fig. 1 Molecular structures of PT (donor) and $IC_{60}BA$ (acceptor).

mismatched alloys.[28–30] However, it is challenging to establish an IB within a semiconductor material and the experimental photoelectric conversion efficiency is relatively low.[31] In order to broadly and efficiently enhance optical nonlinearities, SPRs may be a feasible way. SPRs arise from the coherent oscillations of electrons near the surface of noble metals.[32,33] The coupling of plasmons with excitons and the formation of plexcitons typically cause the enhancement of molecular properties.[34] Employing the plasmonic effect to enhance molecular nonlinear properties, such as nonlinear plexcitons, may be more prominent in solar cells. Fofang *et al.* reported the nonlinear mechanism of plexcitons by studying the exciton–plasmon coupling in *J*-aggregate-Au nanoshell complexes.[35] Manjavacas *et al.* theoretically investigated the nonlinear effects of plexcitons under strong optical pumping.[36] Ovchinnikov *et al.* experimentally observed the nonlinear absorption enhancement of methylene blue based on the plasmonic coupling of Au/SiO_2 core–shell nanoparticles.[37] Furthermore, many studies have proven that nonlinear plasmonic effects are more likely to induce robust electric field enhancement.[38–40] These studies demonstrate the feasibility and prospect of applying the plasmonic-enhanced two-photon absorption (PETPA) method to solar cells, where the TPA properties of photoactive materials may be strongly enhanced though nonlinear plexcitons.

In this work, we theoretically demonstrate the excellent TPA behavior of a PT:$IC_{60}BA$ D–A structure. The photoinduced CT and electron–hole coherence of different excitation processes in TPA are studied. A reasonable PETPA method is employed based on the theoretical framework. Through the plasmonic coupling between Au@Ag core–shell nanorods and an Ag metal film, the enhancement factor can reach up to the order of 10^6, which indicates that the TPA property in the OCS material is increased by 10^6 times. Furthermore, the incident angle or polarization direction is adjusted and the results show that the incident light at a small angle can obtain the most significant plasmonic enhancement. Our research provides theoretical guidance for designing high-efficiency solar cells based on nonlinear plexcitons.

2. Methods

All quantum calculations were performed using Gaussian 16. The ground state geometries of monomer and complex structures were optimized using density functional theory (DFT) with the B3LYP functional and the 6-31 g(d) basis set.[41] The electronic transitions of structures were investigated with time-dependent DFT (TDDFT), the CAM-B3LYP functional, and the 6-31 g(d) basis set.[42] Multiwfn program was used to draw the maps of the transition density matrix (TDM) and charge density difference (CDD).[43]

Two-photon spectroscopy was studied visually by the program developed by Sun and Mu *et al.*[44,45] The full data are obtained from the Gaussian package. The TPA cross-section can be defined as:

$$\sigma_{\mathrm{tp}} = \frac{4\pi^2 a_0^5 \alpha}{15c} \frac{\omega^2 g(\omega)}{{}_{\mathrm{f}}} \delta_{\mathrm{tp}}, \tag{1}$$

where c is the speed of light, Γ_{f} is the lifetime of the final state, a_0 is the Bohr radius, α is the fine structure constant, ω is the energy of the incident light, and $g(\omega)$ expresses the spectral line profile, which is assumed to be a δ function. The transition probability, δ_{tp}, in eqn (1) can be expressed as:

$$\delta_{\mathrm{tp}} = 8 \sum_{\substack{m \neq g \\ m \neq f}} \frac{|\langle f|\mu|m\rangle|^2 |\langle m|\mu|g\rangle|^2}{\left(E_{\mathrm{m}} - \frac{E_{\mathrm{f}}}{2}\right)^2 + \Gamma_{\mathrm{f}}{}^2} (1 + 2\cos^2\theta) + 8 \frac{\left|\Delta\mu_{\mathrm{fg}}\right|^2 |\langle f|\mu|g\rangle|^2}{\left(\frac{E_{\mathrm{f}}}{2}\right)^2 + \Gamma_{\mathrm{f}}{}^2} (1 + 2\cos^2\varphi), \tag{2}$$

where $|g\rangle$ represents the ground state, $|f\rangle$ denotes the final state, and $|m\rangle$ stands for the intermediate state; μ is the electrical dipole moment operator, E_{m} and E_{f} are the excited state and final state energy, and $\Delta\mu_{\mathrm{fg}} = \langle f|\mu|f\rangle - \langle g|\mu|g\rangle$ is the difference between the excited states' permanent dipole moments and that of the ground state; θ and φ are the angles between the vectors $\langle f|\mu|m\rangle$ and $\langle m|\mu|g\rangle$ and between the vectors $\Delta\mu_{\mathrm{fg}}$

 This journal is © The Royal Society of Chemistry 2022

Published on 11 April 2022. Downloaded on 12/26/2025 10:37:54 AM.

and $\langle f|\mu|g\rangle$, respectively. This method is essentially a sum-over-state (SOS) method, which is robust in calculating many nonlinear optical properties.[44,46,47]

The plasmonic-enhanced TPA and electric field distribution of the nanostructure were simulated by the finite-difference time-domain (FDTD) method. The alloy nanorod comprised an Ag shell with a thickness of 5 nm coated on an Au core with a length of 55 nm and a diameter of 10 nm. The thicknesses of the molecular layer and the Ag film are 1.5 nm and 40 nm, respectively, which are arranged on a conductive glass substrate composed of an indium tin oxide (ITO) film and SiO_2. The schematic diagram is shown in Fig. 2. The dielectric constants of Au, Ag and ITO were taken from ref. 48, 49 and 50, respectively, and the dielectric constant of the molecular layer was calculated using the Vienna *ab initio* simulation package (VASP). More details on the FDTD simulations are available in the ESI.†

3. Results and discussion

The foundation of a solar cell material lies in its strong absorption in the visible region. Our previous work has discussed the linear optical performances of PT, $IC_{60}BA$ and their D–A structure in detail.[51] The PT:$IC_{60}BA$ (n = 9) system composed of a PT molecule with a unit number (n) of nine and an $IC_{60}BA$ molecule can well represent the material's performance at the macro level.[51] However, we noticed that, for the shorter molecular chain, the ground state structure of the complex is "semi-circular", which cannot represent the infinite length of the polymer, see the inset in Fig. 3(a). Therefore, we made an improvement by calculating the PT:$IC_{60}BA$ (n = 17) complex structure composed of one PT molecule with n = 17 and two $IC_{60}BA$ molecules, see the inset in Fig. 3(b). Their one-photon absorption (OPA) spectra are similar, proving that our calculations are correct, see Fig. 3. The absorption spectra show that the PT:$IC_{60}BA$ complex has a strong optical absorption from 400 to 500 nm, confirming its feasibility as a photoactive material. A weak redshift of the absorption peak for the longer chain is observed, which is explained in the ESI.†

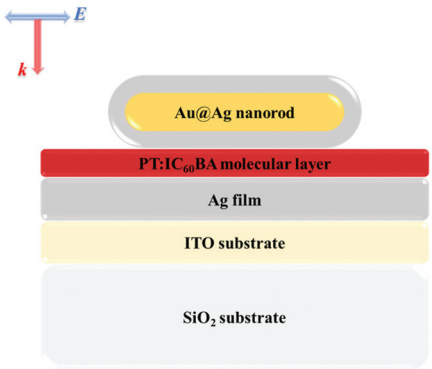

Fig. 2 Schematic diagram of the plasmonic-enhanced TPA in OSCs, where the inset shows the initial light source orientation for all discussions in this paper.

The fast and abundant electron transfer between molecules is particularly important for solar cells based on the D–A system. However, intermolecular CT excited states are generally weak in OPA, which significantly limits the efficiency of solar cells. In the process of TPA, the "three-state term" offers the opportunity for both efficient intermolecular CT and strong optical absorption, simultaneously. One of the origins of the nonlinear properties of PT and $IC_{60}BA$ has been demonstrated owing to the conjugated systems.[52,53] To thoroughly explore the role of TPA in the PT:$IC_{60}BA$ D–A system, we investigated the TPA spectra of donor PT (n = 17) and acceptor $IC_{60}BA$, respectively. Fig. 4(a) shows the TPA spectrum of the donor material. According to the characteristic of TPA, the excitation wavelength should be twice that of OPA. It can be seen that there are strong TPA excited states from 750 to 1000 nm, corresponding to S_2 and S_4 in the OPA spectrum, which are contributed from the "three-state terms" in eqn (2), where $|\langle f|\mu|j\rangle|^2|\langle j|\mu|g\rangle|^2$ and $|\Delta\mu_{fg}|^2|\langle f|\mu|g\rangle|^2$ represent the "three state" and "two state" terms, respectively. Compared with the extremely weak absorption of S_2 and S_4 in the OPA spectrum,[51] these excited states exhibit strong nonlinear optical properties in TPA. The near-infrared TPA cross-section of PT is consistent with previous reports.[54–56] Fig. 4(b) shows the TPA spectrum of

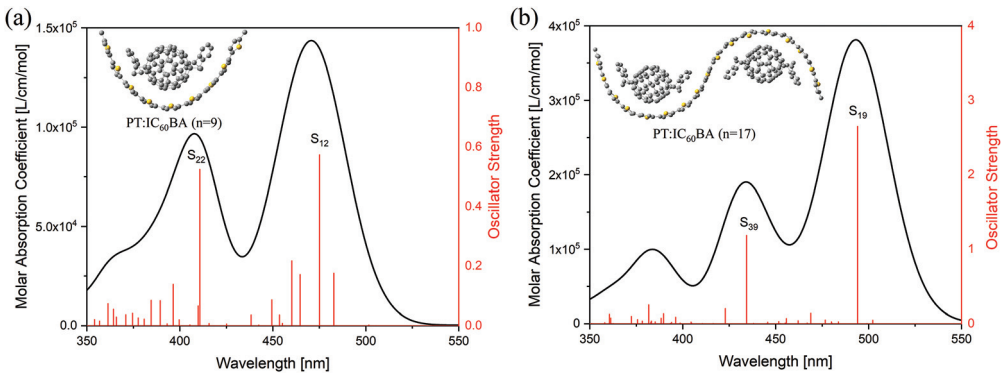

Fig. 3 OPA spectra of (a) PT:$IC_{60}BA$ (n = 9) and (b) PT:$IC_{60}BA$ (n = 17), where the insets show the corresponding structures of the PT:$IC_{60}BA$ complex system.

Published on 11 April 2022. Downloaded on 12/26/2025 10:37:54 AM.

TPA spectrum of PT:IC$_{60}$BA (n=9) can be seen in the Supporting Information.

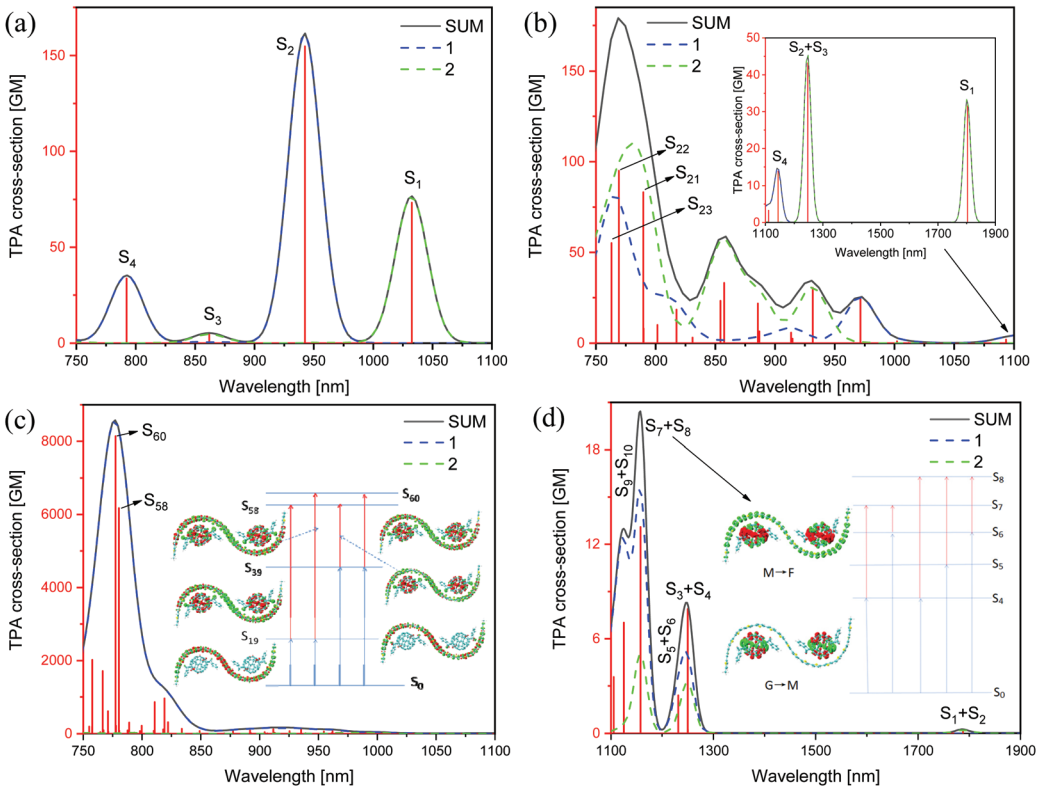

Fig. 4 TPA spectra of (a) donor PT (n = 17) and (b) acceptor IC$_{60}$BA, where the inset shows the one at wavelengths from 1100 to 1900 nm. (c) and (d) TPA spectra of the PT:IC$_{60}$BA complex in different regions, where the inset shows excitations with different transition channels, and the red and green represent electrons and holes, respectively. 1 and 2 are "three-state terms" and "two-state terms", respectively. G, M and F represent the ground, intermediate and final states, respectively.

the acceptor material, and the inset is the one in the long-wavelength region. The acceptor material has strong TPA response from 750 to 800 nm and the σ_{max} value is 94 GM, which is similar to ref. 57. As a whole, the experimental and calculated TPA cross-sections of C_{60}/C_{70} derivatives are in the range of 10^{-49}–10^{-46} cm^4 s per photon (1 GM = 10^{-50} cm^4 s per photon).[46,58,59] For S_1 around 1800 nm, only a "one-step" transition is possible. Note that the S_1 of IC$_{60}$BA has a non-negligible TPA cross-section, which seems unreasonable, because with regard to the nonpolar molecule IC$_{60}$BA,[60] its permanent dipole moment is very small and S_1 is weakly absorbing in the OPA spectrum.[51] According to the "two-state term" formula $|\Delta\mu_{fg}|^2|\langle f|\mu|g\rangle|^2$, its TPA cross-section of S_1 should be small. In fact, IC$_{60}$BA has a larger TPA cross-section in the short-wavelength region, see Fig. S2† in the ESI.† Although the short-wavelength TPA is strong, this is not the range of our study, and S_1 is only a relatively strong peak in the wavelength range we observe. Fig. 4(c) shows that PT:IC$_{60}$BA (n = 17) has a larger TPA cross-section up to 8000 GM compared with the bare IC$_{60}$BA molecule from 750 to 850 nm, which mainly originates from the contributions of S_{58} and S_{60} around 780 nm. In the D–A system, the donor group, thiophene, is an effective "electron bridge" that increases the TPA cross-section.[61,62] Moreover, the long-range excitation from the donor to acceptor could cause a huge TPA cross-section of the complex molecule.[46] As shown in the inset of Fig. 4(c), S_{58} is the strong absorption by the "three-state terms" *via* two transition channels $S_0 \rightarrow S_{19} \rightarrow S_{58}$ and $S_0 \rightarrow S_{39} \rightarrow S_{58}$, and S_{60} is *via* two transition channels $S_0 \rightarrow S_{19} \rightarrow S_{60}$ and $S_0 \rightarrow S_{39} \rightarrow S_{60}$, respectively. Furthermore, the transitions from the ground state to the intermediate states are local excitation on thiophene, since almost all the electrons and holes are localized on the thiophene units (the red and green represent electrons and holes, respectively). For the transitions from the intermediate states to the final states, the maps of CDD show that electrons and holes are distributed on both the donor and acceptor, but it is difficult to analyze the degree of exciton delocalization, which will be discussed later. Fig. 4(d) shows the TPA spectrum of the complex in the region from 1100 to 1900 nm, which is mainly contributed from the acceptor, IC$_{60}$BA. There are two near degenerate strong "three-state term" absorption peaks of S_7 and S_8, and their optical properties show the local excitation of IC$_{60}$BA on the transitions from the ground state to the intermediate states; and on the transitions from the intermediate states to the final states, it is intermolecular CT. The TPA spectrum of PT:IC$_{60}$BA (n = 9) can be seen in the ESI.†

The maps of CDD demonstrate the local excitation from the ground state to the intermediate states at S_{58} and S_{60} shown in Fig. 4(c), in which photoinduced excitons localized in the

 This journal is © The Royal Society of Chemistry 2022

Published on 11 April 2022. Downloaded on 12/26/2025 10:37:54 AM.

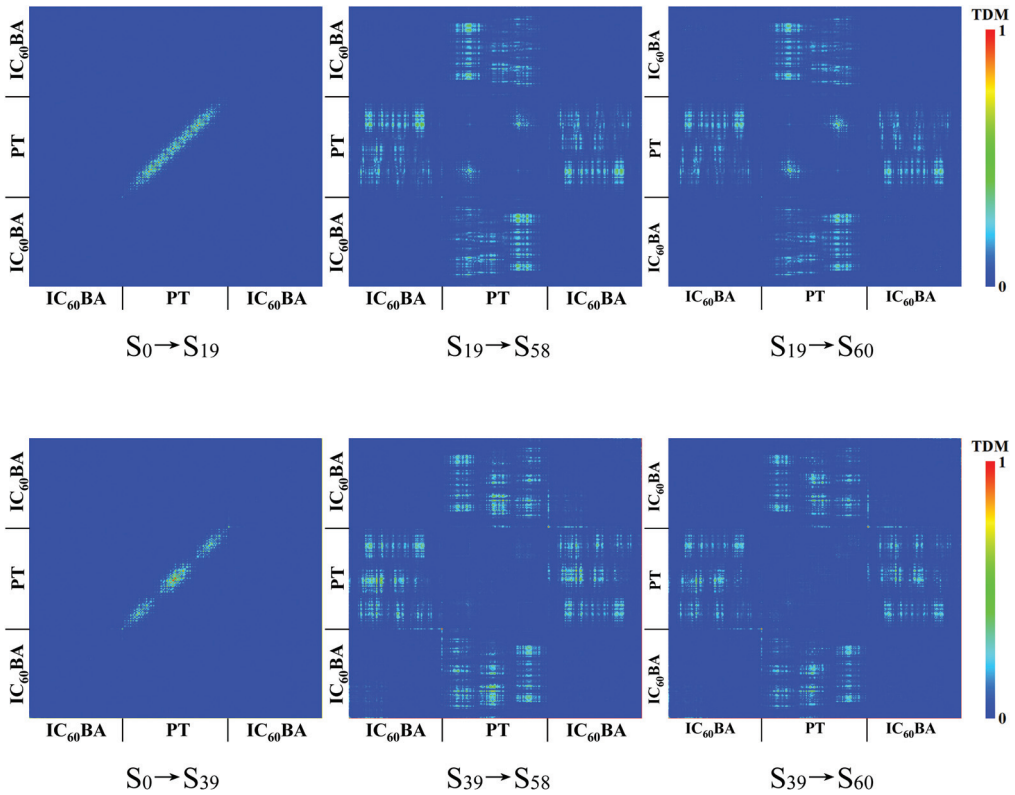

Fig. 5 TDMs of different transition channels. The scale bar stands for the strength of electron–hole coherence.

donor thiophene oligomer. In order to further reveal the degree of exciton delocalization, the TDM is employed, as shown in Fig. 5. It can be found that for the "three-state term" process at S_{58} and S_{60}, the "first step" is the intramolecular local excitation. Electrons and holes form intense bound states due to the Coulomb interaction in adjacent units with larger exciton binding energy, which are typical Frenkel excitons. The large binding energy can facilitate light-harvesting.[63] The "second step" is the intermolecular CT, which generates CT excitons. In general, CT excitons can cause large second-order nonlinear polarizabilities.[64,65] These mixed Frenkel–CT excitons exhibit the properties of both types of contributing states: the Frenkel excitons provide a large oscillator strength, whereas the CT excitons cause a high sensitivity to the external electric field.[65] Actually, hybridized Frenkel–CT exciton states have been used to analyze the TPA spectrum of the *N*,*N*-dimethylaminobenzylidene 1,3-indandione (DMABI) molecule.[66,67] The S_{58} and S_{60} at around 780 nm can simultaneously satisfy the large TPA cross-section and efficient intermolecular CT. Therefore, applying SPRs to enhance the electric field at 780 nm can effectively improve the TPA performance and intermolecular CT of the PT:$IC_{60}BA$ material, which is of great significance to OCS based on this material. More details about TDM and CDD can be seen in the ESI.†

The PT:$IC_{60}BA$ complex molecule is known to have a huge nonlinear response at 780 nm. In a nonlinear optical process such as second harmonic generation (SHG),[68] a nanometal absorbs two low-energy photons resulting in a near-field enhancement with the corresponding frequency, and simultaneously generates a high-energy photon with twice the energy, forming a dual-enhancement of the fundamental and double frequencies. This is a multiple SPR effect,[69] and the enhancement factor (EF) can be estimated as[70]

$$\mathrm{EF} = |M_{\mathrm{in}}|^2 |M_{\mathrm{sc}}|^1, \tag{3}$$

where $|M_{\mathrm{in}}|$ and $|M_{\mathrm{sc}}|$ represent the plasmonic enhancement of the fundamental (incident) and double (scattering) frequencies in TPA, respectively, and $|M| = |E_{\mathrm{local}}/E_{\mathrm{in}}|$, where E_{local} and E_{in} are the local and incident electric fields, respectively. According to eqn (3), the plasmonic nanostructure needs to obtain simultaneously strong E_{local} at both frequencies to maximize the PETPA. When the fundamental and double frequencies correspond to 780 nm and 390 nm in TPA, using metal nanorods is a good choice for such plasmonic-enhanced configurations. This is because the polarization varies, the longitudinal and transverse modes of the nanorods will appear simultaneously, and the SPR peaks shift with the variation of the nanorods' aspect ratio, which facilitate the tuning of the resonance peaks. Considering that solar cells are usually made of metal films as electrodes, we design an Au@Ag nanorod-molecule-Ag film plexciton system and the thickness of the PT:$IC_{60}BA$ molecular layer in the cavity is 1.5 nm. We used Au@Ag nanorods in our calculations due to their strong

Published on 11 April 2022. Downloaded on 12/26/2025 10:37:54 AM.

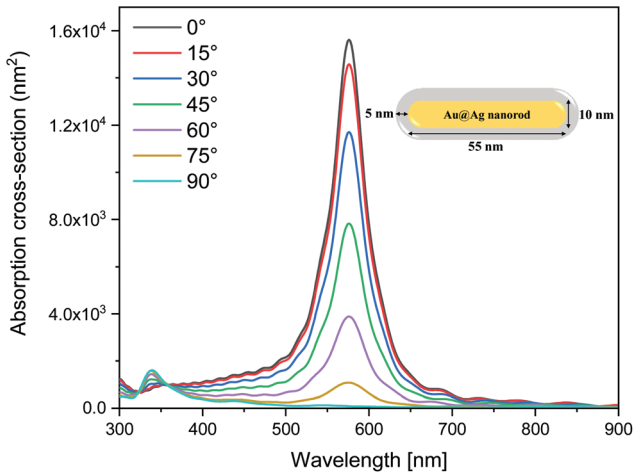

Fig. 6 Absorption spectra of Au@Ag nanorods with different polarization angles (φ).

plasmonic enhancement and easy-tunability of SPR peaks.[70] For metal nanorods, it has been reported that the polarization angle (φ) and incident angle (θ) increase from 0°, the transverse resonance is enhanced and the longitudinal resonance is weakened.[70,71] Fig. 6 shows the absorption spectra of a single Au@Ag nanorod used in our subsequent calculations with various polarizations, and the inset shows the geometrical parameters of the nanorod. The SPR peaks at 580 nm and 340 nm result from the longitudinal and transverse excitations of the nanorod, respectively. When the nanorod is coupled with an Ag film, the plasmonic coupling leads to a redshift in the resonance peaks.[72] The absorption spectra of the coupled structure are shown in the ESI.† Interestingly, the resonance peaks of the coupled structure just agree with the TPA spectroscopy of the PT:$IC_{60}BA$ material. Therefore, this coupled structure can be used to enhance the nonlinear properties of the PT:$IC_{60}BA$ material.

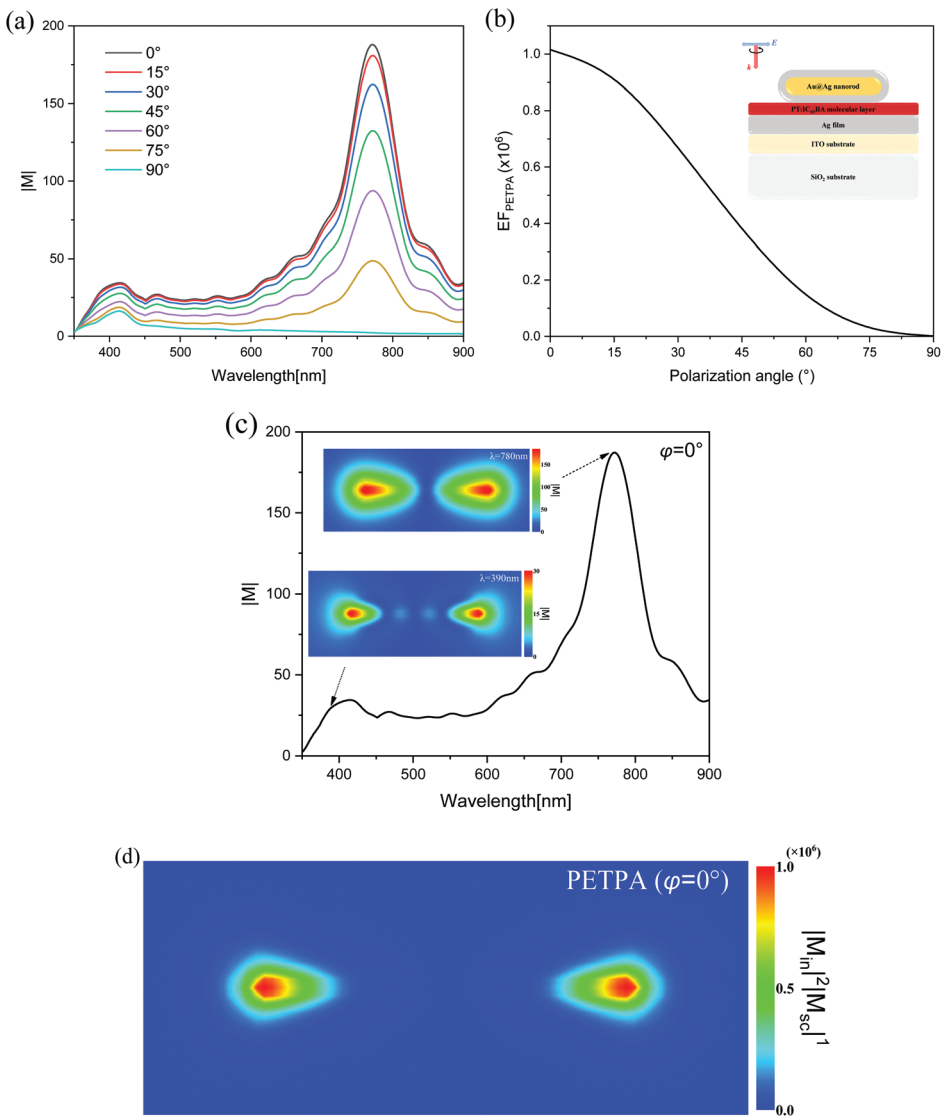

Fig. 7 (a) Plasmonic-enhanced electric field with different φ values. (b) EF of PETPA *versus* φ. (c) The plasmonic-enhanced electric field when φ = 0°, where the insets show electric field distributions. (d) PETPA distribution when φ = 0°.

 This journal is © The Royal Society of Chemistry 2022

Published on 11 April 2022. Downloaded on 12/26/2025 10:37:54 AM.

Fig. 7(a) shows the plasmonic-enhanced electric fields with different φ values in the molecular layer. There are two strong SPR peaks corresponding to the transverse and longitudinal modes of the Au@Ag nanorod at 390 nm and 780 nm, both of which decrease as the φ value increases. The strong electric field at the fundamental and double frequencies can significantly enhance the TPA in the molecular layer. However, the absorption spectra of the single Au@Ag nanorod shows that the transverse resonance will be enhanced as the φ value increases, which is different from the results in Fig. 7(a). Tcherniak *et al.* reported that hot electron–hole pairs can also create surface plasmons causing the transverse and longitudinal modes to be orthogonal to each other.[73] Fig. 7(b) shows the EF of PETPA *versus* φ. When $\varphi = 0°$, the strongest EF can be obtained, and as the φ value increases, the intensity of the EF decreases rapidly. When the polarization direction is perpendicular to the nanorod ($\varphi = 90°$), the enhanced TPA is almost invisible. Fig. 7(c) shows the enhanced electric field when $\varphi = 0°$, in which the maximum EF is obtained. The insets in Fig. 7(c) show the electric field distributions in the molecular layer at 390 and 780 nm. It can be seen that for the fundamental and double frequencies, the plasmons localized at both ends of the nanorod exhibit dipole behavior. Fig. 7(d) shows the distribution of PETPA in the molecular layer. The maximum EF at both ends of the nanorod can reach the order of 10^6, which indicates that the TPA properties can be enhanced about 10^6 times.

It is known that the increase of the polarization angle will lead to an almost linear decrease of the EF in the molecule. When $\varphi = 0°$, we change the incident angle θ, and the

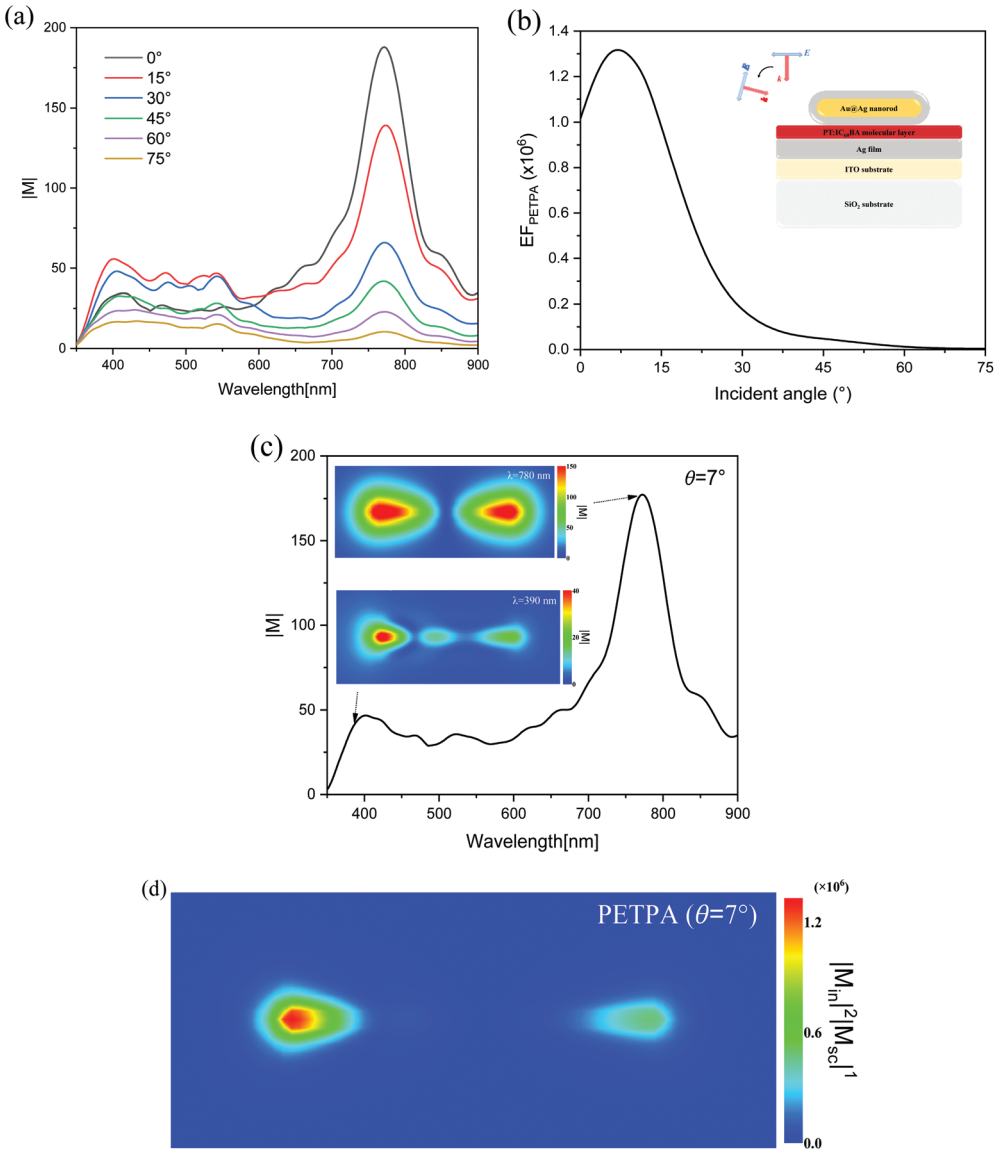

Fig. 8 (a) Plasmonic-enhanced electric field with different θ values. (b) EF of PETPA *versus* θ. (c) The plasmonic-enhanced electric field when $\theta = 7°$, where the insets show electric field distributions. (d) PETPA distribution when $\theta = 7°$.

Published on 11 April 2022. Downloaded on 12/26/2025 10:37:54 AM.

enhanced electric fields with different θ values are shown in Fig. 8(a). At the fundamental frequency of 780 nm, the electric field intensity decreases as the θ value increases. However, at the double frequency of 390 nm, as the θ value increases, the electric field intensity increases at the small θ value. Fig. 8(b) shows the relationship between the EF and θ in the molecular layer. It can be seen that the EF increases first and then decreases, reaching the maximum value around $\theta = 7°$. Also, when changing θ, the overall decreasing trend of the EF is steeper than changing φ. For the maximum PETPA obtained when $\theta = 7°$ and $\varphi = 0°$, the electric field distributions of the fundamental and double frequencies are studied, as shown in the insets of Fig. 8(c). At 780 nm, a slight increase in the incident angle does not result in a drastic decrease for the enhanced electric field. At 390 nm, the electric field distribution varies greatly, and an asymmetric mode appears when the θ value is increased. This is because the change of the incident angle will cause the symmetry to be broken, and there is a decaying oscillation process when the wave vector propagates along the long axis, even the formation of stationary waves. Such a robust plasmon-aggregation behavior at one end usually exhibits better performance and broader applications.[74,75] According to eqn (3), the EF when $\theta = 7°$ and $\varphi = 0°$ is about 1.3 times stronger than that when $\theta = 0°$ and $\varphi = 0°$ in the molecular layer, and the PETPA distribution also exhibits substantial agminated enhancement at one end, as shown in Fig. 8(d). Note that there is another configuration for increasing the incident angle while keeping the polarization angle and rotating the incident light around the longitudinal axis of the nanorod, which can be seen in Fig. S5 in the ESI.†

It is known that the properties of the coupling structure depend greatly on the angle of the light source, but the extent of dependence on different parameters is indefinite, such as the influence on the fundamental and double frequencies, and the dependence of the polarization and incident angles.

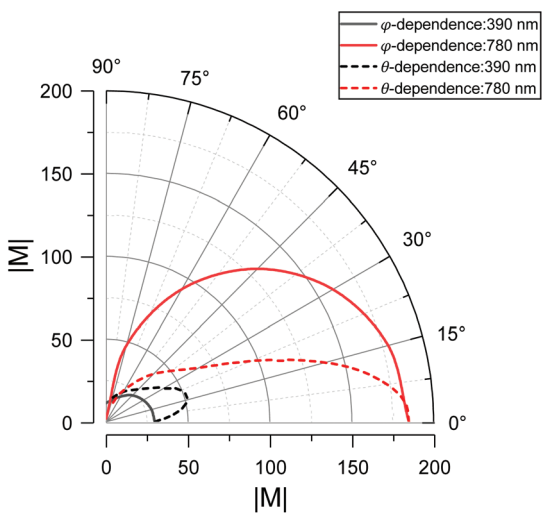

Fig. 9 The electric fields of fundamental and double frequencies in polar coordinates.

To solve this, we compared the extent of angle dependence in polar coordinates. Fig. 9 shows the φ/θ dependence of the fundamental and double frequencies, and the curvature of the arc can indicate the dependence extent. For the fundamental frequency (red), the curvature of the dotted line is larger than the solid line, which means that θ influences the electric field more at the fundamental frequency. For the double frequency (black), the increase of θ will lead to the increase of the electric field, reaching the maximum at 15°. When the θ value increases continuously, the electric field will decrease rapidly compared with φ changes.

4. Conclusion

TPA spectroscopy analyses suggest that a PT:$IC_{60}BA$ complex has a large TPA cross-section. Through the coupling of Au@Ag nanorods and an Ag film, the EF of PETPA in the molecular layer can reach the order of 10^6, which means that its TPA properties can be increased by 10^6 times. Studies on the polarization and incident angle dependence show that the small incident angle can result in a stronger nonlinear plasmonic enhancement. Our results focus on the physical mechanism of nonlinear plexcitons and provide theoretical guidance for the plasmonic-enhanced nonlinear properties of OSC materials.

Conflicts of interest

There are no conflicts to declare.

Acknowledgements

This work was supported by the National Natural Science Foundation of China (91436102 and 11374353) and the Fundamental Research Funds for the Central Universities (06500067).

References

1 L. Cui, S. Zhu and M. Sun, External Electric Field Manipulating Sequential and Super-Exchange Charge Transfer in Donor-Bridge-Acceptor System in Two-Photon Absorption, *Phys. E*, 2021, **134**, 114840.
2 Y. Gong, G.-L. Hou, X. Bi, N. Kuthirummal, A. A. Teklu, J. Koenemann, N. Harris, P. Wei, K. Devera and M. Hu, Enhanced Two-Photon Absorption in Two Triphenylamine-Based All-Organic Compounds, *J. Phys. Chem. A*, 2021, **125**, 1870–1879.
3 A. Farenbruch, D. Fröhlich, D. Yakovlev and M. Bayer, Two-Photon Absorption and Second Harmonic Generation of 1^s Para-and Orthoexcitons in Cu_2o Coupled by a Magnetic Field, *Phys. Rev. B*, 2020, **102**, 115203.
4 M. Kauranen and A. V. Zayats, Nonlinear Plasmonics, *Nat. Photonics*, 2012, **6**, 737–748.

 This journal is © The Royal Society of Chemistry 2022

Published on 11 April 2022. Downloaded on 12/26/2025 10:37:54 AM.

5 N. B. Grosse, J. Heckmann and U. Woggon, Nonlinear Plasmon-Photon Interaction Resolved by K-Space Spectroscopy, *Phys. Rev. Lett.*, 2012, **108**, 136802.
6 S. Palomba and L. Novotny, Nonlinear Excitation of Surface Plasmon Polaritons by Four-Wave Mixing, *Phys. Rev. Lett.*, 2008, **101**, 056802.
7 M. Jablan, Quasiclassical Nonlinear Plasmon Resonance in Graphene, *Phys. Rev. B*, 2020, **101**, 085424.
8 M. Rumi and J. W. Perry, Two-Photon Absorption: An Overview of Measurements and Principles, *Adv. Opt. Photonics*, 2010, **2**, 451–518.
9 M. Göppert-Mayer, Über Elementarakte Mit Zwei Quantensprüngen, *Ann. Phys.*, 1931, **401**, 273–294.
10 W. K. C. Garrett and W. Kaiser, Two-Photon Excitation in Caf_2: Eu^{2+}, *Phys. Rev. Lett*, 1961, **7**, 229–231.
11 J. Lott, C. Ryan, B. Valle, J. R. Johnson III, D. A. Schiraldi, J. Shan, K. D. Singer and C. Weder, Two–Photon 3d Optical Data Storage Via Aggregate Switching of Excimer–Forming Dyes, *Adv. Mater.*, 2011, **23**, 2425–2429.
12 Z. Giedraityte, M. Tuomisto, M. Lastusaari and M. Karppinen, Three-and Two-Photon Nir-to-Vis (Yb, Er) Upconversion from Ald/Mld-Fabricated Molecular Hybrid Thin Films, *ACS Appl. Mater. Interfaces*, 2018, **10**, 8845–8852.
13 Y. Chen and M. Sun, Two-Dimensional Ws_2/Mos_2 Heterostructures: Properties and Applications, *Nanoscale*, 2021, **13**, 5594–5619.
14 T. Rajh, N. M. Dimitrijevic, M. Bissonnette, T. Koritarov and V. Konda, Titanium Dioxide in the Service of the Biomedical Revolution, *Chem. Rev.*, 2014, **114**, 10177–10216.
15 F. Bolze, S. Jenni, A. Sour and V. Heitz, Molecular Photosensitisers for Two-Photon Photodynamic Therapy, *Chem. Commun.*, 2017, **53**, 12857–12877.
16 J. Shi, Q. Guo, Z. Shi, S. Zhang and H. Xu, Nonlinear Nanophotonics Based on Surface Plasmon Polaritons, *Appl. Phys. Lett.*, 2021, **119**, 130501.
17 B. Sharma, R. R. Frontiera, A.-I. Henry, E. Ringe and R. P. Van Duyne, Sers: Materials, Applications, and the Future, *Mater. Today*, 2012, **15**, 16–25.
18 A. Luque and A. Martí, The Intermediate Band Solar Cell: Progress toward the Realization of an Attractive Concept, *Adv. Mater.*, 2010, **22**, 160–174.
19 M. Albota, *et al.*, Design of Organic Molecules with Large Two-Photon Absorption Cross Sections, *Science*, 1998, **281**, 1653–1656.
20 O. Varnavski, X. Yan, O. Mongin, M. Blanchard-Desce and T. Goodson, Strongly Interacting Organic Conjugated Dendrimers with Enhanced Two-Photon Absorption, *J. Phys. Chem. C*, 2007, **111**, 149–162.
21 X. Li, Z. Li and Y.-W. Yang, Tetraphenylethylene-Interweaving Conjugated Macrocycle Polymer Materials as Two-Photon Fluorescence Sensors for Metal Ions and Organic Molecules, *Adv. Mater.*, 2018, **30**, 1800177.
22 T. G. Allen, *et al.*, Highly Conjugated, Fused-Ring, Quadrupolar Organic Chromophores with Large Two-Photon Absorption Cross-Sections in the near-Infrared, *J. Phys. Chem. A*, 2020, **124**, 4367–4378.
23 N. Tsuboya, R. Hamasaki, M. Ito, M. Mitsuishi, T. Miyashita and Y. Yamamoto, Nonlinear Optical Properties of Novel Fullerene–Ferrocene Hybrid Molecules, *J. Mater. Chem.*, 2003, **13**, 511–513.
24 G. Zhao, Y. He and Y. Li, 6.5% Efficiency of Polymer Solar Cells Based on Poly(3-Hexylthiophene) and Indene-C60 Bisadduct by Device Optimization, *Adv. Mater.*, 2010, **22**, 4355–4358.
25 S. Nam, D. Khim, G. T. Martinez, A. Varambhia, P. D. Nellist, Y. Kim, T. D. Anthopoulos and D. D. C. Bradley, Significant Performance Improvement in N-Channel Organic Field-Effect Transistors with C60:C70 Co-Crystals Induced by Poly(2-Ethyl-2-Oxazoline) Nanodots, *Adv. Mater.*, 2021, **33**, 2100421.
26 R. Abbassi, A. Abbassi, M. Jemli and S. Chebbi, Identification of Unknown Parameters of Solar Cell Models: A Comprehensive Overview of Available Approaches, *Renewable Sustainable Energy Rev.*, 2018, **90**, 453–474.
27 N. Ahsan, N. Miyashita, M. M. Islam, K. M. Yu, W. Walukiewicz and Y. Okada, Two-Photon Excitation in an Intermediate Band Solar Cell Structure, *Appl. Phys. Lett.*, 2012, **100**, 172111.
28 A. Martí, E. Antolín, C. R. Stanley, C. D. Farmer, N. López, P. Díaz, E. Cánovas, P. G. Linares and A. Luque, Production of Photocurrent Due to Intermediate-to-Conduction-Band Transitions: A Demonstration of a Key Operating Principle of the Intermediate-Band Solar Cell, *Phys. Rev. Lett.*, 2006, **97**, 247701.
29 N. López, L. A. Reichertz, K. M. Yu, K. Campman and W. Walukiewicz, Engineering the Electronic Band Structure for Multiband Solar Cells, *Phys. Rev. Lett.*, 2011, **106**, 028701.
30 T. Li and M. Dagenais, Non-Resonant Below-Bandgap Two-Photon Absorption in Quantum Dot Solar Cells, *Appl. Phys. Lett.*, 2015, **106**, 171101.
31 Y. Okada, *et al.*, Intermediate Band Solar Cells: Recent Progress and Future Directions, *Appl. Phys. Rev.*, 2015, **2**, 021302.
32 T. Klar, M. Perner, S. Grosse, G. Von Plessen, W. Spirkl and J. Feldmann, Surface-Plasmon Resonances in Single Metallic Nanoparticles, *Phys. Rev. Lett.*, 1998, **80**, 4249.
33 O. Nicoletti, F. de La Peña, R. K. Leary, D. J. Holland, C. Ducati and P. A. Midgley, Three-Dimensional Imaging of Localized Surface Plasmon Resonances of Metal Nanoparticles, *Nature*, 2013, **502**, 80–84.
34 N. T. Fofang, T.-H. Park, O. Neumann, N. A. Mirin, P. Nordlander and N. J. Halas, Plexcitonic Nanoparticles: Plasmon–Exciton Coupling in Nanoshell–J-Aggregate Complexes, *Nano Lett.*, 2008, **8**, 3481–3487.
35 N. T. Fofang, N. K. Grady, Z. Fan, A. O. Govorov and N. J. Halas, Plexciton Dynamics: Exciton–Plasmon Coupling in a J-Aggregate–Au Nanoshell Complex Provides a Mechanism for Nonlinearity, *Nano Lett.*, 2011, **11**, 1556–1560.

Published on 11 April 2022. Downloaded on 12/26/2025 10:37:54 AM.

36 A. Manjavacas, F. J. García de Abajo and P. Nordlander, Quantum Plexcitonics: Strongly Interacting Plasmons and Excitons, *Nano Lett.*, 2011, **11**, 2318–2323.
37 O. V. Ovchinnikov, M. S. Smirnov, T. A. Chevychelova, A. I. Zvyagin and A. S. Selyukov, Nonlinear Absorption Enhancement of Methylene Blue in the Presence of Au/Sio2 Core/Shell Nanoparticles, *Dyes Pigm.*, 2022, **197**, 109829.
38 L. Sun, Y. Chen and M. Sun, Exploring Nonemissive Excited-State Intramolecular Proton Transfer by Plasmon-Enhanced Hyper-Raman Scattering and Two-Photon Excitation Fluorescence, *J. Phys. Chem. C*, 2022, **126**, 487–492.
39 G. Spektor, D. Kilbane, A. Mahro, M. Hartelt, E. Prinz, M. Aeschlimann and M. Orenstein, Mixing the Light Spin with Plasmon Orbit by Nonlinear Light-Matter Interaction in Gold, *Phys. Rev. X*, 2019, **9**, 021031.
40 L. Cui, R. Li, T. Mu, J. Wang, W. Zhang and M. Sun, In Situ Plasmon-Enhanced Cars and Tpef for Gram Staining Identification of Non-Fluorescent Bacteria, *Spectrochim. Acta, Part A*, 2022, **264**, 120283.
41 J. Tirado-Rives and W. L. Jorgensen, Performance of B3lyp Density Functional Methods for a Large Set of Organic Molecules, *J. Chem. Theory Comput.*, 2008, **4**, 297–306.
42 T. Yanai, D. P. Tew and N. C. Handy, A New Hybrid Exchange–Correlation Functional Using the Coulomb-Attenuating Method (Cam-B3lyp), *Chem. Phys. Lett.*, 2004, **393**, 51–57.
43 T. Lu and F. Chen, Multiwfn: A Multifunctional Wavefunction Analyzer, *J. Comput. Chem.*, 2012, **33**, 580–592.
44 X. Mu, J. Wang and M. Sun, Visualization of Photoinduced Charge Transfer and Electron–Hole Coherence in Two-Photon Absorption, *J. Phys. Chem. C*, 2019, **123**, 14132–14143.
45 M. Sun, J. Chen and H. Xu, Visualizations of Transition Dipoles, Charge Transfer, and Electron-Hole Coherence on Electronic State Transitions between Excited States for Two-Photon Absorption, *J. Chem. Phys.*, 2008, **128**, 064106.
46 S. Chakrabarti and K. Ruud, Intermolecular Interaction-Controlled Tuning of the Two-Photon Absorption of Fullerene Bound in a Buckycatcher, *J. Phys. Chem. A*, 2009, **113**, 5485–5488.
47 X. Zhou, W.-Q. Li, B. Shao and W. Q. Tian, Nonlinear Optical Properties of Fullerene C96 (D3d) and Related Heterofullerenes, *J. Phys. Chem. C*, 2013, **117**, 23172–23177.
48 P. B. Johnson and R.-W. Christy, Optical Constants of the Noble Metals, *Phys. Rev. B: Solid State*, 1972, **6**, 4370.
49 E. D. Palik, *Handbook of Optical Constants of Solids*, Academic press, 1998, vol. 3.
50 R. J. Moerland and J. P. Hoogenboom, Subnanometer-Accuracy Optical Distance Ruler Based on Fluorescence Quenching by Transparent Conductors, *Optica*, 2016, **3**, 112–117.
51 Y. Chen, Y. Cheng and M. Sun, Physical Mechanisms on Plasmon-Enhanced Organic Solar Cells, *J. Phys. Chem. C*, 2021, **125**, 21301–21309.
52 S. A. Jenekhe, S. K. Lo and S. R. Flom, Third–Order Nonlinear Optical Properties of a Soluble Conjugated Polythiophene Derivative, *Appl. Phys. Lett.*, 1989, **54**, 2524–2526.
53 J. D. Perea, *et al.*, Combined Computational Approach Based on Density Functional Theory and Artificial Neural Networks for Predicting the Solubility Parameters of Fullerenes, *J. Phys. Chem. B*, 2016, **120**, 4431–4438.
54 M. M. Oliva, J. Casado, J. T. L. Navarrete, S. Patchkovskii, T. Goodson, M. R. Harpham, J. S. Seixas de Melo, E. Amir and S. Rozen, Do [All]-S,S'-Dioxide Oligothiophenes Show Electronic and Optical Properties of Oligoenes and/or of Oligothiophenes?, *J. Am. Chem. Soc.*, 2010, **132**, 6231–6242.
55 S. Pascal, S. David, C. Andraud and O. Maury, Near-Infrared Dyes for Two-Photon Absorption in the Short-Wavelength Infrared: Strategies Towards Optical Power Limiting, *Chem. Soc. Rev.*, 2021, **50**, 6613–6658.
56 M. A. Ramírez-Gómez, *et al.*, Physicochemical and Luminescent Properties of Copolymers Composed of Three Monomers: Polythiophenes Based on 3-Hexylthiophene and 3,4-Ethylenedioxythiophene, *Int. J. Polym. Sci.*, 2017, **2017**, 1918602.
57 X. Ouyang, H. Zeng and W. Ji, Synthesis, Strong Two-Photon Absorption, and Optical Limiting Properties of Novel C70/C60 Derivatives Containing Various Carbazole Units, *J. Phys. Chem. B*, 2009, **113**, 14565–14573.
58 X. Zhou, A.-M. Ren and J.-K. Feng, Theoretical Investigation on the Two-Photon Absorption of C60, *J. Mol. Struct.: THEOCHEM*, 2004, **680**, 237–242.
59 S. Jeon, *et al.*, Linear and Nonlinear Optical Properties of Photoresponsive [60]Fullerene Hybrid Triads and Tetrads with Dual Nir Two-Photon Absorption Characteristics, *J. Phys. Chem. C*, 2013, **117**, 17186–17195.
60 T. Ameri, T. Heumüller, J. Min, N. Li, G. Matt, U. Scherf and C. J. Brabec, Ir Sensitization of an Indene-C60 Bisadduct (Icba) in Ternary Organic Solar Cells, *Energy Environ. Sci.*, 2013, **6**, 1796–1801.
61 H. Zhou, F. Zhou, S. Tang, P. Wu, Y. Chen, Y. Tu, J. Wu and Y. Tian, Two-Photon Absorption Dyes with Thiophene as Π Electron Bridge: Synthesis, Photophysical Properties and Optical Data Storage, *Dyes Pigm.*, 2012, **92**, 633–641.
62 M. R. Harpham, Ö. Süzer, C.-Q. Ma, P. Bäuerle and T. Goodson, Thiophene Dendrimers as Entangled Photon Sensor Materials, *J. Am. Chem. Soc.*, 2009, **131**, 973–979.
63 M. Knupfer, Exciton Binding Energies in Organic Semiconductors, *Appl. Phys. A*, 2003, **77**, 623–626.
64 D. S. Chemla, *Nonlinear Optical Properties of Organic Molecules and Crystals V1*, Elsevier, 2012, vol. 1.
65 M. Hoffmann, K. Schmidt, T. Fritz, T. Hasche, V. M. Agranovich and K. Leo, The Lowest Energy Frenkel and Charge-Transfer Excitons in Quasi-One-Dimensional Structures: Application to Meptcdi and Ptcda Crystals, *Chem. Phys.*, 2000, **258**, 73–96.
66 S. Jur?enas, Exciton Spectroscopy in Polar Molecular Films and Crystals, *Phys. Scr.*, 1999, **T79**, 159.
67 S. Jursenas, A. Gruodis, G. Kodis, M. Chachisvilis, V. Gulbinas, E. A. Silinsh and L. Valkunas, Free and Self-Trapped Charge-Transfer Excitons in Crystals of Dipolar Molecules of N,N-Dimethylaminobenzylidene 1,3-Indandione, *J. Phys. Chem. B*, 1998, **102**, 1086–1094.

 This journal is © The Royal Society of Chemistry 2022

Published on 11 April 2022. Downloaded on 12/26/2025 10:37:54 AM.

68 J. Butet, P.-F. Brevet and O. J. F. Martin, Optical Second Harmonic Generation in Plasmonic Nanostructures: From Fundamental Principles to Advanced Applications, *ACS Nano*, 2015, **9**, 10545–10562.
69 D. V. Voronine, Z. Zhang, A. V. Sokolov and M. O. Scully, Surface-Enhanced Fast Cars: En Route to Quantum Nano-Biophotonics, *Nanophotonics*, 2018, **7**, 523–548.
70 X. Mi, Y. Wang, R. Li, M. Sun, Z. Zhang and H. Zheng, Multiple Surface Plasmon Resonances Enhanced Nonlinear Optical Microscopy, *Nanophotonics*, 2019, **8**, 487–493.
71 Y. Huang, Y. Fang and M. Sun, Remote Excitation of Surface-Enhanced Raman Scattering on Single Au Nanowire with Quasi-Spherical Termini, *J. Phys. Chem. C*, 2011, **115**, 3558–3561.
72 J. J. Mock, R. T. Hill, A. Degiron, S. Zauscher, A. Chilkoti and D. R. Smith, Distance-Dependent Plasmon Resonant Coupling between a Gold Nanoparticle and Gold Film, *Nano Lett.*, 2008, **8**, 2245–2252.
73 A. Tcherniak, S. Dominguez-Medina, W.-S. Chang, P. Swanglap, L. S. Slaughter, C. F. Landes and S. Link, One-Photon Plasmon Luminescence and Its Application to Correlation Spectroscopy as a Probe for Rotational and Translational Dynamics of Gold Nanorods, *J. Phys. Chem. C*, 2011, **115**, 15938–15949.
74 S. Zhang, H. Wei, K. Bao, U. Håkanson, N. J. Halas, P. Nordlander and H. Xu, Chiral Surface Plasmon Polaritons on Metallic Nanowires, *Phys. Rev. Lett.*, 2011, **107**, 096801.
75 Y. Fang, Z. Li, Y. Huang, S. Zhang, P. Nordlander, N. J. Halas and H. Xu, Branched Silver Nanowires as Controllable Plasmon Routers, *Nano Lett.*, 2010, **10**, 1950–1954.